Numerical and Experimental Study of Inverse Diffusion LPG-Air Flames Pulsation

Mahmoud Magdy*, Mahmoud Kamal, Ashraf Mostafa Hamed, Ahmed Eldein Hussin and W. Aboelsoud

Department of Mechanical Power Engineering, Faculty of Engineering, Ain Shams University, Abdo Basha, El Sarayat St., 1, Cairo, Egypt
E-mail: mahmoudtaha9080@yahoo.com
**Corresponding Author*

Received 23 March 2021; Accepted 26 August 2021;
Publication 06 October 2021

Abstract

This study uses Ansys 16 commercial package to investigate an accurate numerical model that can trace the flame shape from inverse diffusion combustion of LPG with a focus on the effect of air pulsation on the combustion characteristics. The simulation is based on solving the energy, mass and momentum equations. The large eddy simulation turbulence model and the non-premixed combustion model are used to simulate the pulsating combustion reaction flows in a cylindrical chamber with an air frequency of 10,20,50,100 and 200 rad/sec. The numerical results are in great agreement with the experimental results in the flame shape and the temperature distribution along the combustion chamber in both pulsating and non-pulsating combustion. Diffusion combustion responds positively to pulsating combustion and increases mixing in the reaction zone. Increasing the air frequency increases the temperature fluctuations, the peak turbulent kinetic energy and maximum velocity magnitude, respectively, by 27.3%, 300%, and 200%. Increasing the Strouhal number to 0.23 shortens the flame by 40% and

European Journal of Computational Mechanics, Vol. 30_2–3, 169–196.
doi: 10.13052/ejcm2642-2085.30232

reduces nitric oxide and carbon monoxide by 12% and 40%, respectively, including an environmentally friendly combustion product. The maximum average temperature dropped from 1800 K to 1582 K with a very homogeneous temperature distribution along the combustion chamber which is very important for furnaces.

Keywords: Pulsating combustion, CFD, diffusion flames, large eddy simulation (LES).

1 Introduction

There are a lot of techniques used in combustors to increase coherent turbulence structures. Pulsating combustion is an attractive technology that was first demonstrated by Rayleigh [1] and has been used since 1970, in various applications, for example, boilers, heat exchangers, dryers, etc. [2] where high combustion efficiency and low toxic components of the combustion gases is necessary [3]. The interaction of the acoustic field with the combustion reactants increases the turbulence, mixing rates and enhances the heat and mass transfer rates [4]. Pulsating combustion produces zones of intense mixing of combustion components in the flow, which promotes complete combustion while reducing fuel consumption, increasing heat transfer and reducing pollutant emissions [5]. The inlet velocity fluctuations not only generated vortices flame area when the flame wrapped around them but also caused cusps and even large-scale flame annihilation events [6]. The frequency of oscillations and the amplitude of the unsteady flow are used to control these vortices in Helmholtz pulse combustor to enhance the convective heat transfer coefficient [7]. Increasing the acoustic fluctuations amplitude increases the combusting efficiency up to the quenching limit, also increasing the Strouhal number enhances the mixing between reactants [8]. Increasing the amplitude of the central fluctuations increases the size of the vortices, which shortens and widens the flame [9]. Pulsating air velocity could either lift-off the flames or reattached already lifted flames due to the effect of the generating vortex rings which help to increase flow mixing at the burner exit [10]. Increasing air supply free stream turbulence intensity significantly decreases NO formation in the flame [11]. Pulse combustors can be divided into two main categories valve-less pulse combustors passive control with flow area enlargement and valved pulse combustors active control with mechanical membrane or rotary valves [12]. Herein, the frequency of

air is controlled experimentally by DC motor to drive a rotary valve and numerically by UDF to simulate pulsation on Ansys 16. DC motor speed is used to control the frequency of air pulsation [13]. The acoustic fluctuations on LPG combustion were generated using a cam which move a piston up and down to enhance turbulent kinetic energy on diffusion flame and noticed that the flames oscillate in 'bulk flickering' [14]. Benelli [15] studied Lennox boiler based on a Helmholtz-type mechanically-valved pulse combustor using CFD and achieve a great similarity of sinusoidal pressure and temperature fluctuations with experimental work. Mahmoud Magdy [16] studied the effect of air pulsation on the flame shape on Harwell furnace and investigated a validated model which could predict combustion variables. A lot of researchers used LES instead of RANS models to simulate turbulent combustion because its great accuracy [17, 18]. The effects of chemical dynamics and turbulent diffusion obtained using the probability density function (PDF) model are in good agreement with the experiments, while the results using other models have a significant difference. The PDF model is also used to predict the process of formation of NO, which also corresponds well with the experimental data [19]. The PDF model is used to investigate high swirling effect on non-premixed confined natural gas flame and achieve a favourably prediction with experimental results [20]. Using LES turbulence model with PDF models is the best computational way to investigate turbulent combustion parameters but have proved to be computationally very demanding [21, 22]. The combustion of fuel surrounded by air is called normal combustion. Herein, the air is surrounded by fuel which is denoted by inverse combustion [23]. The experimental data are used to validate simulation results and the main conclusions of pulsating combustion are based on large eddy simulation [24]. The main object of current research is to investigate a very accurate model with ANSYS fluent 16 could track pulsating flames experimental results. A secondary result is a numerical study on the effect of fuel fluctuations on the following variables (velocity, temperatures, turbulent kinetic energy, NO, CO and CO_2).

2 Methodology

ANSYS-fluent 16 is used to model the pulsating flow within the same combustion chamber used experimentally by the Hamed test rig [13] to verify a high agreement model with the experimental results at the following boundary conditions in Table 1.

Table 1 Inlet boundary conditions

Inlet boundary conditions	LPG	AIR
Axial velocity (m/s)	0.028–0.1	1.7
Re (Reynolds number)	1500–5079	1673
Air-fuel ratio	16:1 and 5:1	–
Frequency rad/s	–	10,20,50,100 and 200
Oxygen mass fraction	–	0.2315
Nitrogen mass fraction	–	0.7685
propane mass fraction	0.6	–
Butane mass fraction	0.4	–

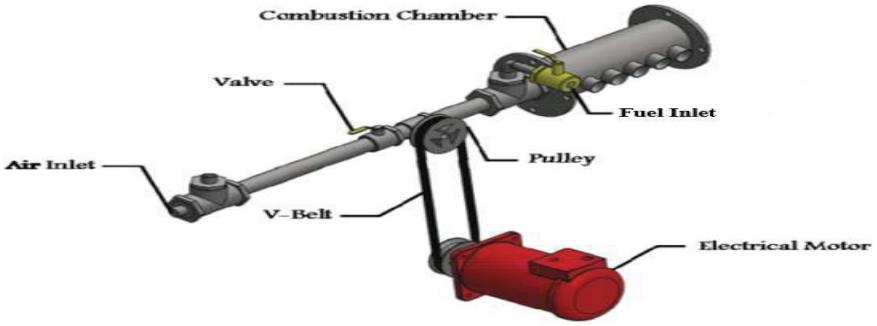

Figure 1 Test rig.

2.1 Test Rig

This test rig was previously used [13] to investigate the effect of air pulsation on the flame. Acoustic fluctuations are driven by a DC motor that rotates a rotary valve. The speed of the DC motor controls the frequency of the air inlet. The air is in the middle and surrounded by the fuel (inverse flame combustion) as shown in Figure 1. The velocity of the air and the fuel is measured with two rotameters representing the amplitude of the air frequency. An s-type thermocouple with a probe diameter of 0.25 mm was used to measure the temperature of the flame. The data acquisition system is used to save the temperature on an excel sheet. This excel sheet is used to validate numeric data. A Nikon digital camera with 2560 $\times$ 1920 pixels and a shutter speed of 1/4000 seconds is used for flame shape comparison. The digital camera was placed opposite the holes of the thermocouple in front of the glass part of the combustion chamber.

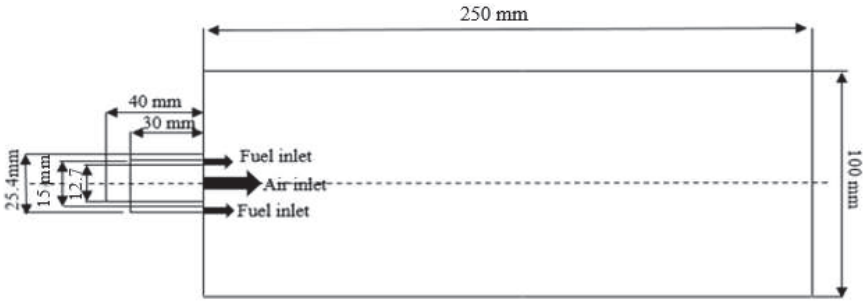

Figure 2 Combustion chamber drawing.

2.2 Computational Domain

A 3D combustion cylinder was drawn with the same dimensions used experimentally. The combustion chamber has 100 mm diameter and 250 mm length. It is connected from the left side by two tubes inside each other. The inside is a circular air inlet with 12.7 mm diameter and the outside is an annular fuel inlet with 25.4 mm outer diameter and 15 mm inner diameter. The other side of the combustion cylinder is the exhaust as shown in Figure 2.

2.3 Computational Grid Details and Test

Ansys fluent is not a simple program just to plot the computational domain, define input boundary conditions, and then start calculating. It is very sensitive to many factors (mesh quality, exact boundary conditions, solution methods, computational models and relaxation factors) [25]. Significant effort must be made to obtain a high-quality mesh with converged residuals. Mesh test is applied by increasing the number of elements and comparing them. The test is performed to obtain the minimum number of elements that achieve approximately the same flow characteristics in order to minimize computational cost, especially with the LES turbulence model [26]. The wall dimensionless factor y^+ can be calculated from the following equation [27].

$$y^+ = \frac{yu_\tau}{v}, \tag{1}$$

The mesh resolution required to properly resolve wall boundary layers in LES, is typically reported as $y^+ = 1$. Grid test is performed at 7, 9 and 12 million elements under the same boundary conditions with 200 rad/s air frequency. The results for 9M and 12.8M $y^+ < 1$, but 7M $y^+ > 1$ therefore it is rejected. The 12.8M element is more accurate and can predict vortices

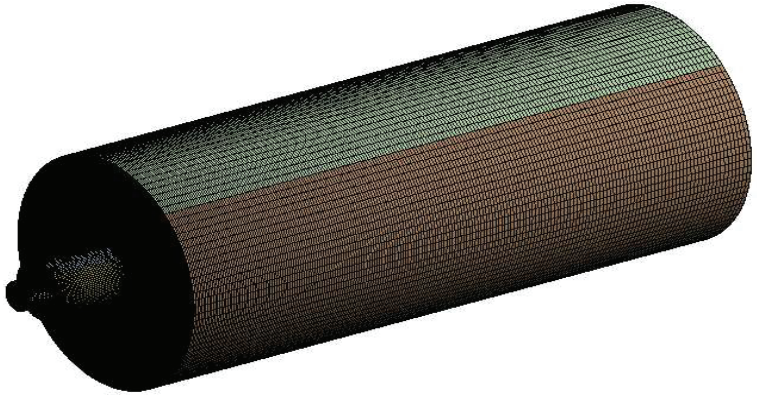

Figure 3 The combustion chamber mesh shape.

smaller than 9M but the solution doesn't change significantly with the refined mesh. Figure 4 represents the temperature changes during combustion time. The temperature is measured at two points, axially at (0,0.02,0) m and radially at (0,0.02, 0.03) m. In Figure 4, there is great similarity between the calculated axial and radial temperatures for both meshes, but the time required to calculate the same case will double when 12M elements are selected, so 9M will be chosen to reduce computational costs. The following data was obtained in Ansys meshing as shown in Figure 3. Advanced size function on curvature, relevance centre high, transition slow, span angle centre fine, min. size 0.322 mm, max face size 4.77 mm, max size 5 mm, growth rate 1.2, minimum edge length 1.15 mm, nodes 9153764, elements 9092250, average aspect ratio 17, average skewness 3.9466 e-2, orthogonal quality 0.99517.

2.4 Governing Equations

The main governing equations used in solving the problem [27] is explained as following.

The equation for conservation of mass, or continuity equation, can be written as follows:

$$\frac{\partial \rho}{\rho t} = \nabla \cdot (\rho \vec{v}) \tag{2}$$

Conservation of momentum in an inertial (non-accelerating) reference frame is described by

$$\frac{\partial}{\partial t}(\rho \vec{v}) + \nabla \cdot (\rho \vec{v} \vec{v}) = -\nabla p + \nabla \cdot (\overline{\overline{\tau}}) + \rho \vec{g} + \vec{F} \tag{3}$$

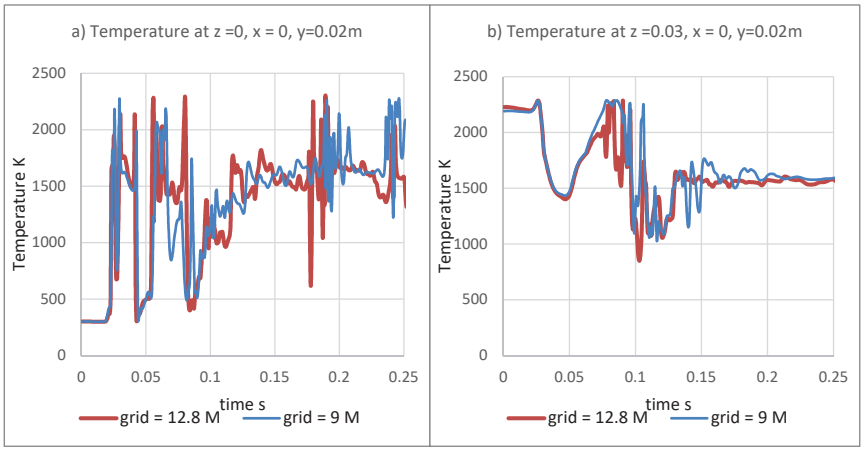

Figure 4 Temperature with time at 9, 12.8 M grids (a) centreline (b) radial.

Burke [28] and Bilger [29] suggested a closure (Non-premixed combustion model) based on mixture fraction (Z) for turbulent diffusion flames with these assumptions.

- Separate streams for fuel and oxidizer (diffusion flames).
- Species diffusion coefficients are equal.
- Suitable for turbulent flows as turbulent diffusion overwhelms.
- Unity Lewis number.
- Flow Mach number is low.
- Species transport equations can be reduced to a single equation for conserving scalar, mixture fraction (Z or f).
- For mixture fraction equation, the reaction source terms cancel out since elements are conserved in chemical reactions.

The energy equation for the non-adiabatic non-premixed combustion Model [29]

$$\frac{\partial}{\partial t}(\rho H) + \nabla \cdot (\rho \vec{v} H) = \nabla \left(\frac{K_t}{C_P} \nabla H \right) + S_h \tag{4}$$

Mixture fraction conservation equation for non-premixed combustion [28]

$$\frac{\partial}{\partial t}(\rho \overline{f}) + \nabla \cdot (\rho \vec{v} \overline{f}) = \nabla \left(\frac{\mu_l + \mu_t}{\sigma_t} \nabla \overline{f} \right) + S_m + S_{user} \tag{5}$$

Conservation equation for the mixture fraction variance for non-premixed combustion

$$\frac{\partial}{\partial t}\left(\rho\overline{f'^2}\right)+\nabla\cdot\left(\rho\vec{v}\overline{f'^2}\right)=\nabla\left(\frac{\mu_l+\mu_t}{\sigma_t}\nabla\overline{f'^2}\right)+C_g\mu_t\left(\nabla\overline{f}\right)^2$$

$$-C_d\rho\frac{\varepsilon}{K}\overline{f'^2}+S_{user}- \tag{6}$$

Where $\sigma_t = 0.85$, Cg = 2.86 and $\mathrm{C_d} = 2.0$.

For Large Eddy Simulations, the transport equation is not solved for the mixture fraction variance. Instead, it is modelled as

$$\overline{f'^2}=C_{var}L_s^2\left|\nabla\overline{f}\right|^2 \tag{7}$$

Turbulence equations for large eddy simulation

The eddy-viscosity is modelled by

$$\mu_{t=}L_s^2|\overline{S}| \tag{8}$$

The mixing length is calculated by

$$L_s=\min(kd,c_s\triangle) \tag{9}$$

$$|\overline{s}|=\sqrt{2S_{ij}S_{ij}} \tag{10}$$

2.5 Solver Settings

ANSYS CFD solvers are based on the finite volume method. Partial differential equations are discretized into a system of algebraic equations which are then solved numerically [27] with the main following settings. The dual-processor parallel solution is used in the HP z800 workstation. Pressure-based solver is chosen because density-based is normally only used with higher Mach numbers. LES (kinetic energy transport model) is used with the following model constants as $\mathrm{Cf_{var}}$ equals 0.5, Energy Prandtl number, Wall Prandtl number and PDF Schmidt number equal 0.85. Energy equation and non-premixed combustion model are activated. Chemical equilibrium, non-adiabatic and inlet diffusion are chosen. LPG is used as fuel type with molecular weight equals 0.6 for propane and 0.4 for butane and then calculate the PDF of the combustion model. $\mathrm{NO_x}$ equation is activated in the non-premixed combustion model.

2.5.1 Solution method

Pressure velocity coupling is selected as following (Scheme PISO, Skewness correction = 1, Neighbor correction = 1). Spatial discretization is selected as following (gradient = least squares cell based, pressure = PRESTO, momentum = bounded central differencing, sub grid kinetic energy = second order upwind, pollutant NO = second order upwind, energy = second order upwind, mean mixture fraction = second order upwind). Bounded second order implicit is selected for transient formulation and convergence criteria is assumed when the residual values are less than 10^{-6}.

2.5.2 Solution control

Under relaxation factors are selected lower than 0.7 to stabilize the solution [27]. The relaxation factors are selected as following pressure = 0.5, density = 0.7, body forces = 1, momentum = 0.3, sub grid kinetic energy = 0.7, turbulent viscosity = 0.5, pollutant number = 1, energy = 0.5.

2.6 Boundary Condition

Boundary conditions have a significant impact on the solution so they must be defined precisely [30]. The fuel inlet velocity is 0.1 and 0.028 m/sec. The inlet air velocity varies sinusoidally over time. Five frequencies are used with cycle time and Strouhal number as shown in Table 2 where D is air inlet diameter = 12.7 mm and u is air inlet velocity = 1.7 m/sec. Air inlet velocity was written in c code as shown in Figure 5 and interpreted in Ansys fluent

Table 2 Cycle time and Strouhal number at different frequencies

Frequencies	f = 10 rad/s	f = 20 rad/s	f = 50 rad/s	f = 100 rad/s	f = 200 rad/s
Cycle time	0.628 s	0.314 s	0.125 s	0.0628	0.0314
St = fD/u	0.011	0.023	0.059	0.11	0.23

```
#include "udf.h"

DEFINE_PROFILE(sinusoidal_Air_velocity, thread, position)
{
face_t f;
real t = CURRENT_TIME;
begin_f_loop(f, thread)
{
F_PROFILE(f, thread, position) = 0.85 + 0.85*sin(200*t);
}
end_f_loop(f, thread)
}
```

Figure 5 Air velocity c code.

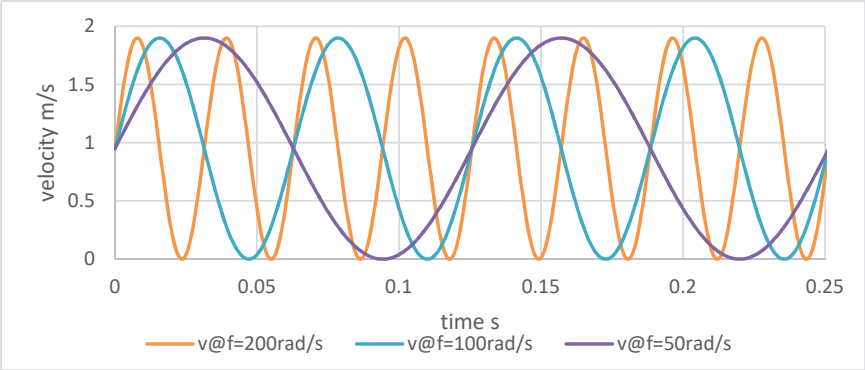

Figure 6 Inlet air velocity profile at different frequencies.

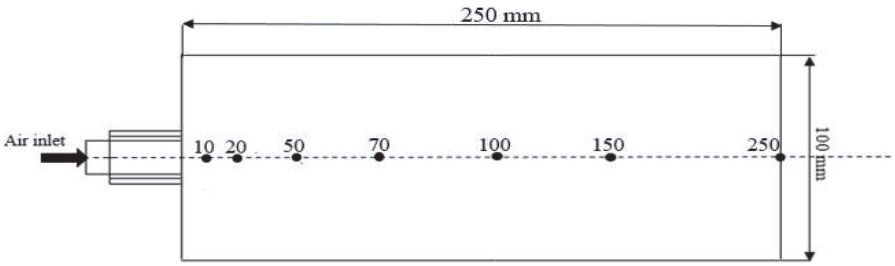

Figure 7 Calculation axial points.

using UDF as shown in Figure 6. Wall of combustion chamber is defined as a stationary wall with no slip. The combustion chamber exhaust is defined as outlet pressure volume = 0 Pa.

2.7 Post Processing

Fluent monitors are used to save the results of T, v, NO, CO and CO_2 at different axial points on the center line (10, 20, 50, 70, 100, 150, 250) mm as shown in Figure 7. In calculation activities, changes in temperature contours are saved over time to create solution animations.

2.8 Time Step Test

Time step size is an important parameter in transient simulations. Time step should be small to resolve the true solution results. The minimum time step Δt required for the flow to travel through the cell with the largest edge

Table 3 The time needed to solve the same problem with different time step

Time Step Size Milliseconds	0.1	0.2	0.6
No of time steps to calculate 0.3 second of combustion	3000	1500	500
Total number of iterations (time step ×35)	105000	52500	17500
Time of calculations (1 minute per iteration)	105000 min	52500 min	17500 min
Number of days	72 days	36 days	12 days

length Δx and the local mean velocity U is calculated by the following equation [27].

$\Delta t = \Delta x/2U = 5/ (2 \times 1.7 \times 1000) = 0.0014$ seconds, the time step should be specified smaller than 0.0013 seconds. Three values for applying the time step test (0.0001–0.0002–0.0006) seconds were determined and compared. As shown in Figure 8, decreasing the time step size increases the detail of the vortices generated by the pulse combustion. Although reducing the time step is effective in solving the vortices it has a very bad effect on computational cost as shown in Table 3. The investigations will take two months to solve one frequency with a time step of 0.0001 s, so the time step of 0.0006 s was chosen.

Each case is applied by the z800 workstation with dual Intel Xeon X5675 processors, 3.1GHz cache, and 32GB RAM using Ain Shams licenses. The Courant number is often used to estimate a time step. The Courant number must be less than 1 for LES.

$$\text{Courant number} = \frac{\text{characteristic flowvelocity} \times \triangle t}{\text{Tybical cell size}}$$

$$= \frac{1.7 \times 0.0006}{0.005} = 0.204 \leq 1$$

Time step of 0.0006 seconds achieves courant number less than 1 and the same main flow characteristics. In Figure 8, the time step test was performed at the same time = 2.5 e-2 sec. It is the end of one pulse cycle at a frequency of 200 rads/sec without any changes in either timesteps.

3 Results and Discussion

3.1 Time Trace of Air Pulsation

In Figure 9, the inverse combustion temperature contours are shown. The following contours represents 8 cycles of pulsating combustion of LPG with

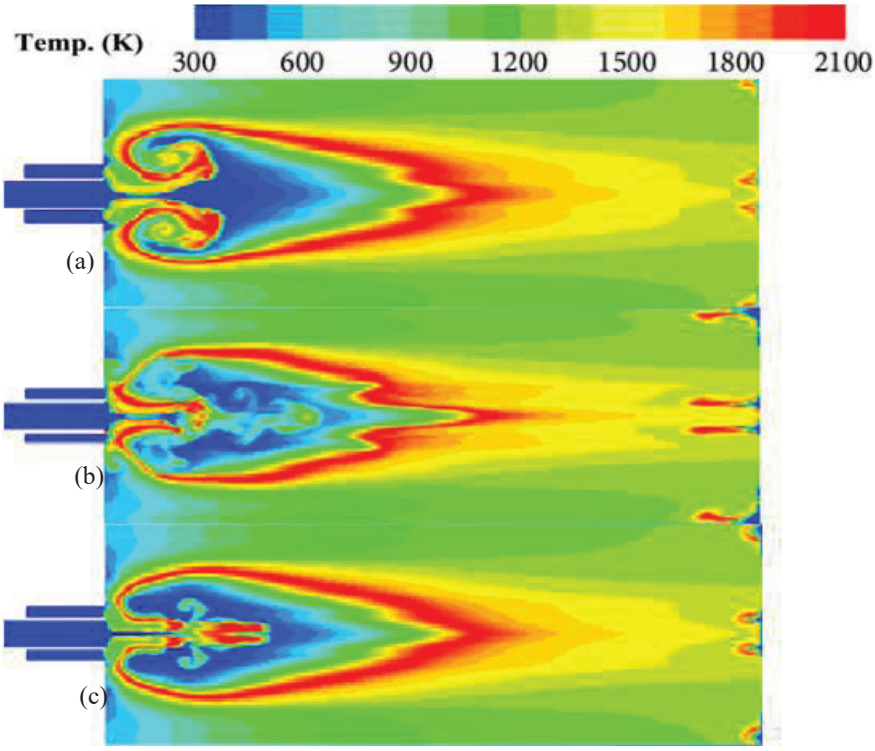

Figure 8 Temperature contour of time step test (a) $\Delta t = 0.0001$ s, (b) $\Delta t = 0.0002$ s, (c) $\Delta t = 0.0006$ s.

air velocity = 1.7 m/s changing sinusoidally with air frequency = 200 rad/s and fuel velocity = 0.028 m/s. The cycle time is 0.0314 seconds so the total combustion time is $8 \times 0.0314 = 0.2512$ seconds. Each cycle was divided into 50 timestep to track the effect of sinusoidal air velocity changes on temperature. In Figure 9 (a) the shape of the initial flame without the effect of the pulse is presented. At the end of the first cycle (b) a small vortex and a small backflow of air are produced at the outlet. The second cycle produces a new vortex of larger dimensions that begins to push the vortices of the first cycle toward the exhaust (C). At the beginning of the third cycle (d) there are a lot of vortices in the sides of the combustion chamber. The final form of pulsating combustion can be observed at the beginning of the fourth cycle (e) which continues to repeat for the end of the 8 cycles (f). The clearest effect of pulse combustion in these lines was to reduce flame length by 40% approximately and have complete combustion at 150 mm.

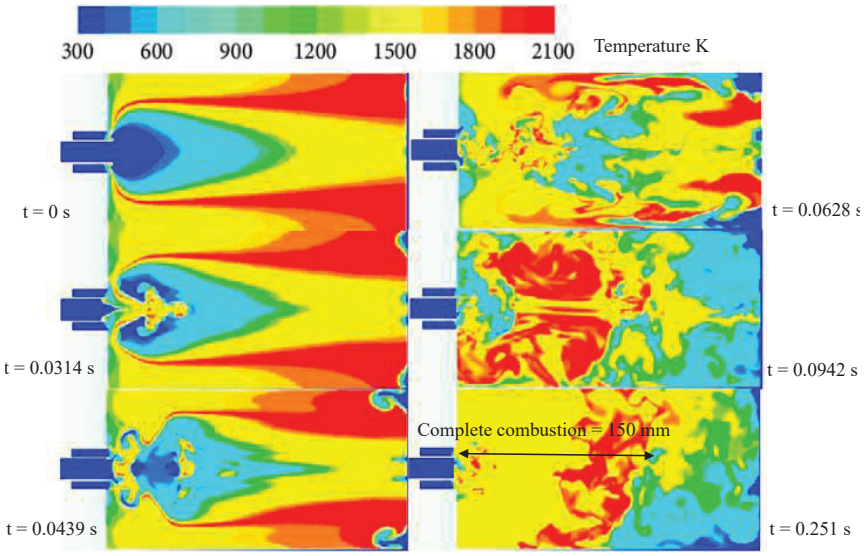

Figure 9 Temperature contour of time step test (a) t = 0 s, (b) t = 0.0314 s, (c) t = 0.0439 s, (d) t = 0.0628 s, (d) t = 0.0439 s, (e) t = 0.0628 s.

3.2 Validation

Validation is mainly based on the comparison of the experimentally measured temperature using thermocouples and flame images taken by a Nikon camera with numerical results in both pulsating and non-pulsating combustion. Numerical simulation of combustion with fine mesh testing, time step testing and convergent residuals can be an effective method for pulse combustion prediction. The convergence criteria were based on the assumption that the residual values of all equations were less than 10^{-6} as shown in Figure 10. The comparison was made under the same boundary conditions, air velocity 1.7 m/s at frequency of 200 rad/s and fuel velocity 0.028 m/s. A great similarity is achieved between the temperature contours and the flame images as shown in Figure 11. In Figure 11(a) the non-premixed flame expands without a pulse and shortens in Figure 11(b) with excitation as the increasing turbulent kinetic energy affects the reaction zone size [31]. In Figure 12, a comparison has been applied between the temperature measured experimentally in the laboratory and the numerical values investigated in pulsating and non-pulsating combustion. The numerical results of the temperature distribution along the combustion chamber are in great agreement with the experimental results in both pulsating and non-pulsating combustion.

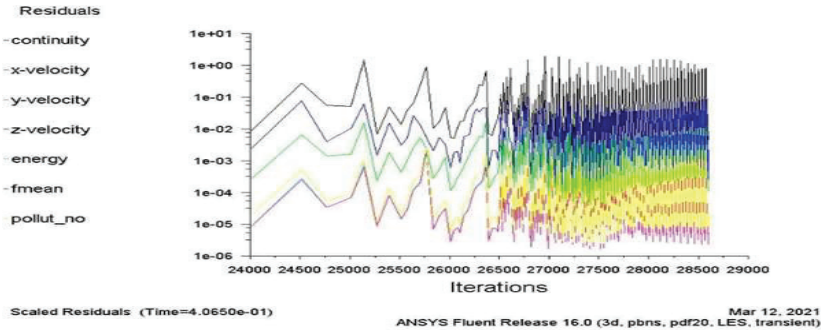

Figure 10 Variation of the residual plot.

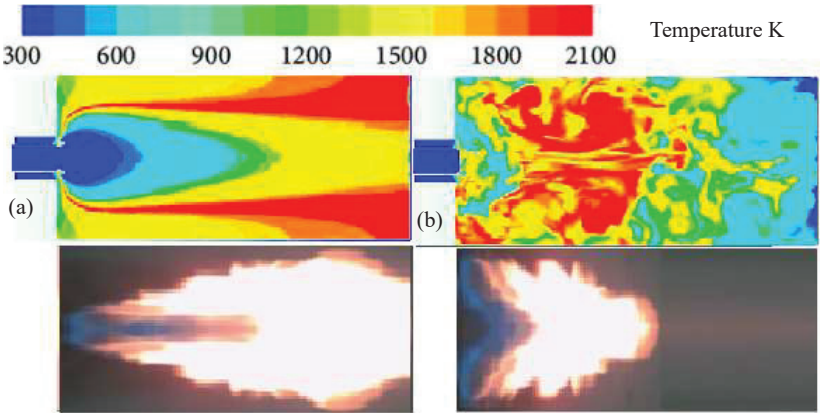

Figure 11 Experimental and numerical flame shape comparison.

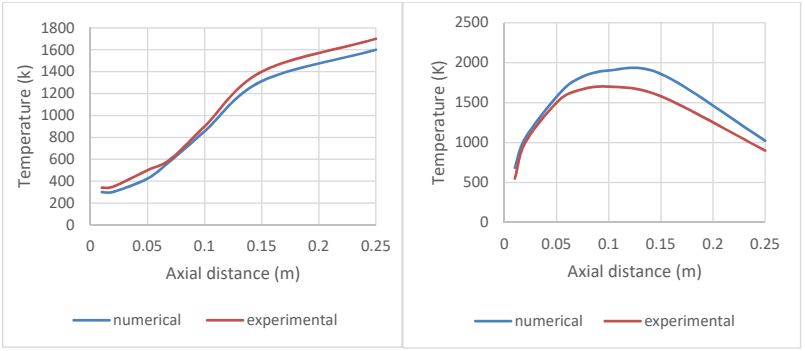

Figure 12 Experimental and numerical temperature comparison.

3.3 Effect of Frequency on Temperature

Acoustic combustion has a significant effect on the flame shape. The pulsating air velocity produces vortices that increase the air-fuel mixing. Well air fuel mixing reduces the length of the diffusion flame so that the average temperature is shifted towards the jetting nozzle. The instantaneous temperatures in pulsating combustion change quickly and therefore it is difficult to compare them, so the average temperatures are used for comparison. The average temperature increases with increasing air frequency at distances from 0.01 m to 0.1 m and decreases at distances from 0.15 m to 0.25 m. In fuel velocity equals 0.028 m/s, the average flame temperature shifts more towards the jetting nozzle. Pulsating combustion increases the homogeneous distribution of temperature in the combustion chamber. Shifting the flame towards the jet nozzle closer to the fresh air helps to cool the flame. At an air frequency of 200 rad/s, the average temperature obtained is between a maximum of 1582 K and a minimum of 1147 K but at 10 rad/s the temperature was obtained between a maximum of 1800 K and a minimum of 576 K as shown in Figure 13. The average maximum temperature has fallen from 1800 K. to 1582 K due to increasing frequency, which has a significant role in reducing the mass percentage of pollutants. Improving air frequency increases temperature fluctuations by 27.3% as shown in Figures 14 and 15. Temperature fluctuations also respond faster.

3.4 Effect of Frequency on Velocity Magnitude

The air inlet velocity changes sinusoidally over time as shown in Figure 6. When the air velocity increased to 1.7 m/s, the pressure in the middle

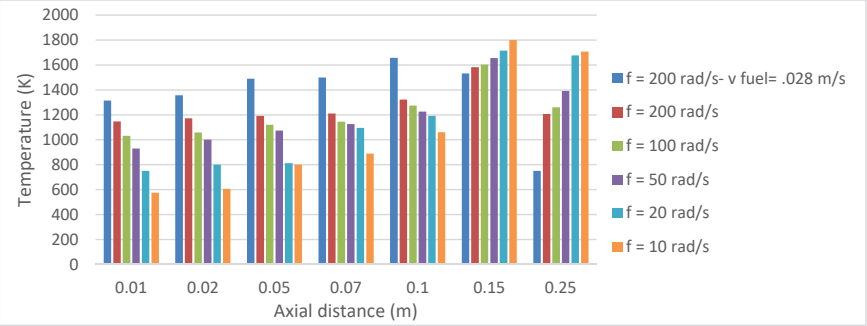

Figure 13 Effect of air frequency of average temperature at axial distance.

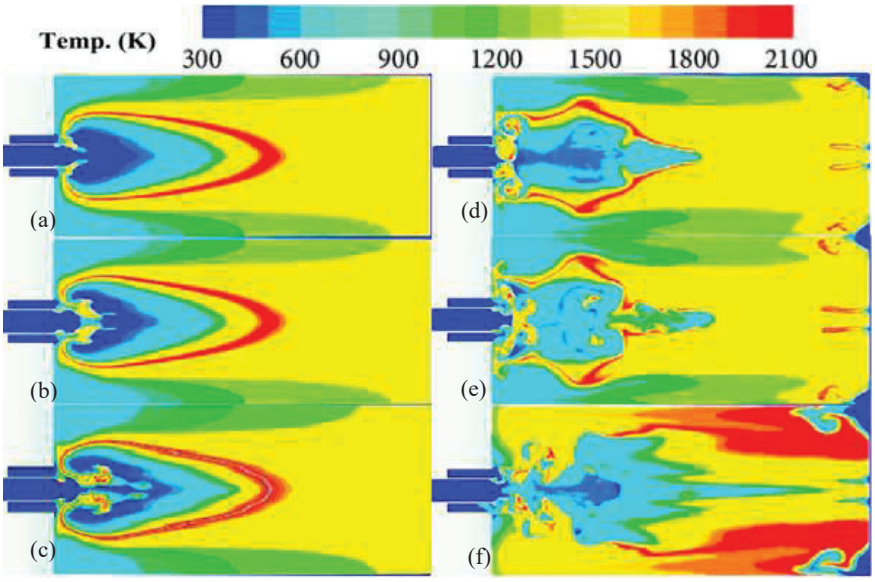

Figure 14 Temperature contour at t = 0.05 s for (a) f = 10 rad/s, (b) f = 20 rad/s, (c) f = 50 rad/s, (d) f = 100 rad/s, (e) f = 200 rad/s (f) f = 200 rad/s with V_{fuel} = 0.028 m/s.

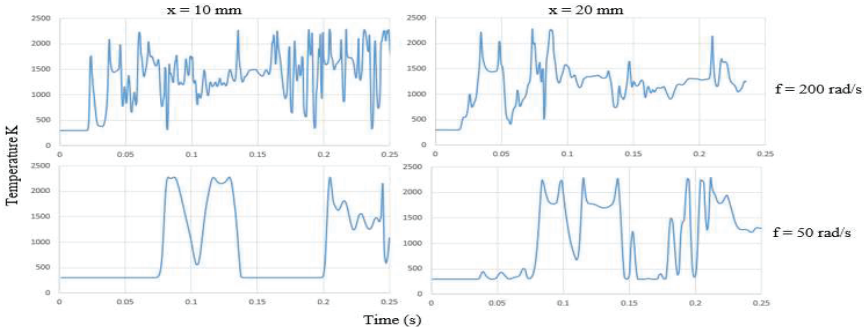

Figure 15 Effect of air frequency on temperature with time at x = 10 mm and 20 mm.

increased tangentially directing the fuel velocity. When the air velocity decreased to 0 m/s, the pressure dropped and absorbed the fuel velocity to the middle. These differences in pressure values generate vortices that increase the shear between the combustion layers and increase the fuel-air mixing. Temporal variations in combustion include hotspots (entropic fluctuations) or vorticity perturbations that generate pressure waves. Increasing the air velocity frequency causes more pressure waves to be generated which increase the

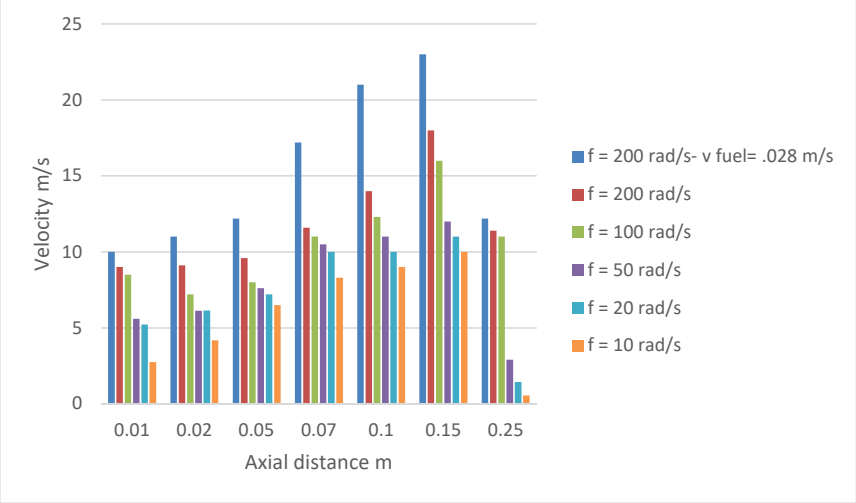

Figure 16 Air Frequency and maximum velocity during Operation at axial distance.

maximum velocity produced as shown in Figure 16. The maximum velocity generated at 0.15 m axial from the jetting nozzle. Increasing the air velocity frequency increases the maximum velocity of combustion products by 200%. High velocities of combustion products can dry materials directly without the need for nozzles or atomizers that require expensive pumps [32]. The oscillating gas stream leaving the combustion chamber can act as an excellent dispenser and atomizer [3].

3.5 Effect of Frequency on Turbulent Kinetic Energy (TKE)

The air pulsation generates vortices and a change in pressure which enhances the interaction between the air-fuel at the hot spots. These hotspots showed a positive increase in velocity gradient which served as a productive center for turbulence. Since the turbulent kinetic energy indicates how strongly large and small scales interact while the entrainment rate reflects how fast the reactants provide for combustion [33]. Increasing the intensity of atmospheric air turbulence leads decrease the NO mass fraction [34]. The maximum turbulent kinetic energy is obtained at y = 0.15 m where the maximum average temperature is obtained. At fuel velocity equals 0.028 m/s, the maximum turbulent kinetic energy increased by 133% at the same frequency of 200 rad/sec. Increasing the air frequency from 20 rad/sec to 200 rad/sec enhances the turbulence intensity by 300% as shown in Figure 17.

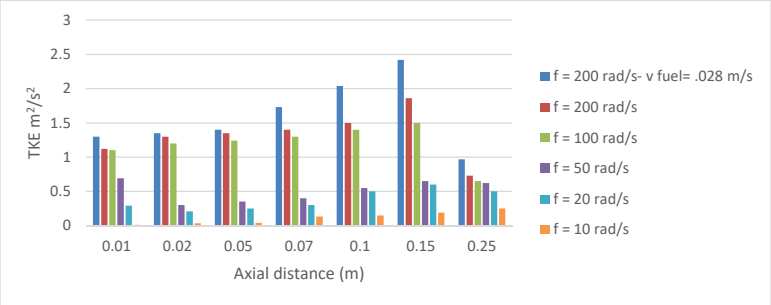

Figure 17 Air Frequency and maximum TKE during Operation at axial distance.

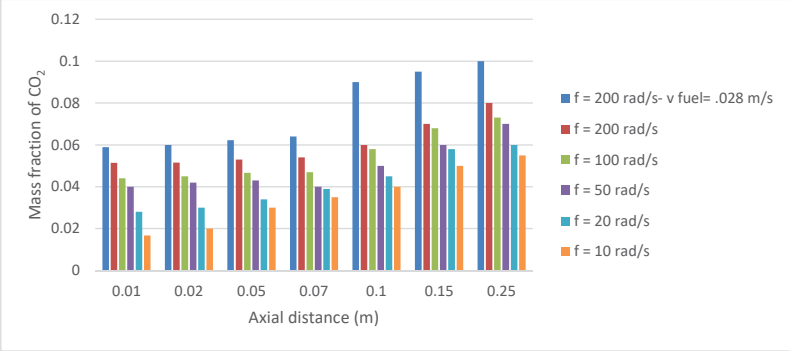

Figure 18 Effect of air frequency of average Mass fraction of CO_2 at axial distance.

3.6 Effect of Frequency on Carbon Dioxide (CO_2)

The mass fraction of carbon dioxide is formed mainly in the flame with a high concentration there, and disperses into the whole combustion chamber [33]. Complete combustion products increased due to high turbulence kinetic energy and good air fuel mixing. The average mass fraction of carbon dioxide increases with increasing frequency at all points as shown in Figure 18. This increase correlates with the increase in oxygen consumption in chemical reactions. The maximum average mass fraction of carbon dioxide produced at the exhaust. The mass fraction of carbon dioxide was shifted to nozzle because the length of the flame was reduced by 40%.

3.7 Effect of Frequency on Carbon Monoxide (CO)

Carbon monoxide is an odorless, colorless, tasteless, and flammable gas that is slightly less dense than air. It is toxic to animals that use hemoglobin as

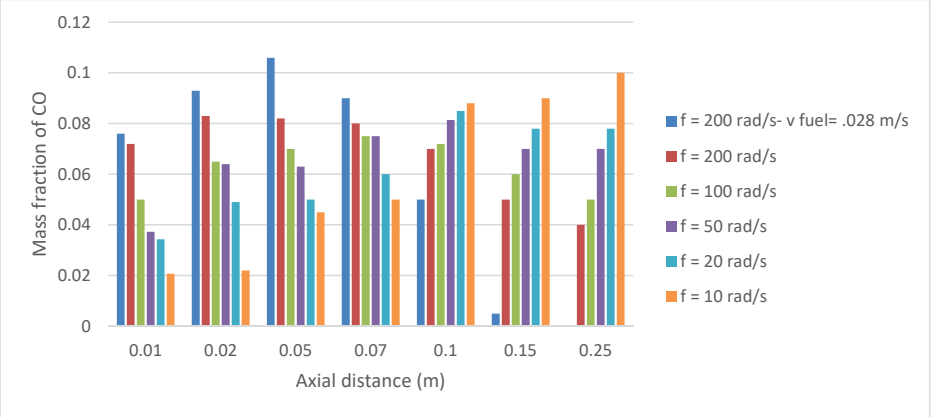

Figure 19 Effect of air frequency of average Mass fraction of CO at axial distance.

an oxygen carrier. In the atmosphere, it is spatially variable, short-lived and has a role in the formation of ground-level ozone [34]. The increase in air pulsation enhances the complete combustion of LPG so that the mass fraction of carbon monoxide is decreased. The average mass fraction of CO decreases with increasing air frequency near the exhaust at a distance from 0.15 mm to 0.25 mm by 40% and increases near the nozzle at a distance from 0.01 mm to 0.1 mm as shown in Figure 19. The main reason for the increase in the mass fraction of carbon dioxide near the jet nozzle is that increasing the air frequency reduces the diffusion length. This region contains small chemical reactions before the pulsating and after the excitation, the chemical reactions occurred mainly at this axial distance. When the fuel velocity is 0.028 m/s, the mass fraction of CO can be neglected at an axial distance from 0.1 mm to 0.25 mm.

3.8 Effect of Frequency on Nitric Oxide (NO)

One of the most important tasks in combustion technology is to reduce pollutants so that the mass fraction of nitrogen oxide must be accurately predicted. Air frequency change is used to control nitrogen oxide emissions in the combustion process. Thermal NOx, Fuel NO_x and Prompt NO_x are the main sources of NO_x in combustion processes. Thermal NO_x is the most relevant source of nitrogen oxide formation during combustion which is highly temperature dependent. The latter two are less important for this study because they are little influenced by flame temperature. The thermal

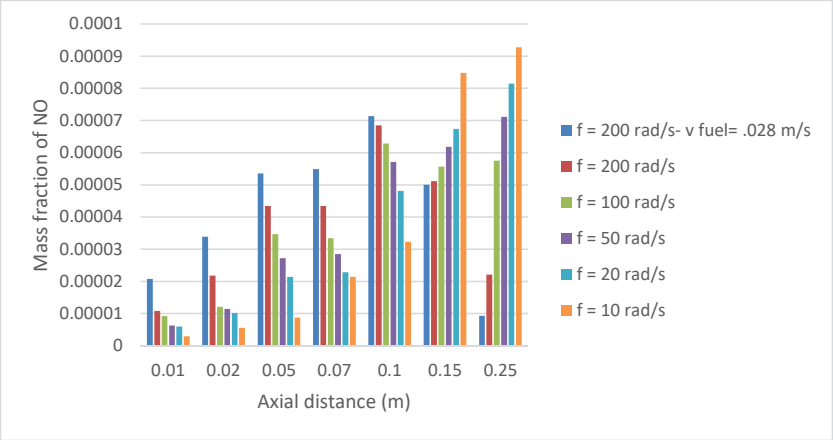

Figure 20 Effect of air frequency of average Mass fraction of NO at axial distance.

mechanism of NO is described by the oxidation of atmospheric N_2 in high-temperature regions of the flame. The formation of NO_x is directly related to the time that nitrogen remains in the reaction zone, the flame temperature and the position of the maximum temperature [35]. In Figure 20, the average mass fraction of NO decreases with increasing air frequency near the exhaust at a distance of 0.15 mm to 0.25 mm and increases near the jetting nozzle from 0.01 mm to 0.1 mm. It was also shown before the NO production was transferred towards the nozzle because chemical reactions occurred in this area due to the pulsation. Increasing air turbulence intensity decreases NO formation [36]. At exhaust, the mass fraction of NO decreases by 12% due to the reduction of the maximum average temperature from 1800 K to 1582 K and the enhancement of the turbulence intensity by 300%. Air injection time reduction also reduces the potential for NO production.

4 Conclusion and Future Recommendations

A CFD numerical model was examined using Ansys Fluent 16 and validated with experimental temperature results. The 3D model with the LES turbulent model and non-premixed combustion model achieved reasonable agreement results with the experimental data. The model presented in this work studies the main effect of air velocity frequency change on combustion variables. The acoustic fluctuations of the flame caused vortices and a more homoganizatin of the temperatures inside the combustion chamber. The maximum

average temperature dropped from 1,800 K to 1,582 K and the flame length decreased by 40%. The inclusion of lowering the temperature also reduced the mass fraction of NO by 12%. Increasing the air frequency from 20 rad/sec to 200 rad/sec enhances the intensity of the turbulence by 300%. On the other hand, the CO mass fraction decreases by 40% as a result of achieving good mixing and complete combustion. The velocity of combustion products increase of 200% at 0.15 m axial from the jet nozzle so that the pulsating combustion chamber can function as an excellent dispenser and atomizer. An interesting next step in this paper will be to use a 3D model to investigate the effect of air inlet port geometric shape on pulsating flames. The use of pulsating combustion with swirlers can also be studied. This model can be used to examine important new effects of pulsation on soot and radiation.

Nomenclature

Re	=	Reynolds number $\equiv$ ratio of inertial forces to viscous forces (dimensionless)
∇	=	Gradient Operator
y^+	=	dimensionless distance from the wall
μ	=	Dynamic viscosity (cP, Pa-s, lbm /ft-s)
$\vec{v}$	=	Overall velocity vector (m/s, ft/s)
f	=	frequency (rad/sec)
ρ	=	Density (kg/m^3)
$\vec{F}$	=	Force vector (N)
H	=	Total enthalpy (energy/mass, energy/mole)
S	=	Total entropy
$\vec{g}$	=	Gravitational acceleration (m/s2, ft/s2); standard values = 9.80665 m/s2, 32.1740 ft/s2
ℓ, l, L	=	Length scale (m, cm, ft, in)
K	=	Equilibrium constant
S_{ij}	=	Mean rate-of-strain tensor (s –1)
T	=	Temperature (K)
t	=	Time (s)
σ	=	Surface tension (kg/m, dyn/cm, lbf/ft)
C_P	=	Heat capacity at constant pressure, volume (J/kg-K)
P	=	Pressure (Pa, atm, mm Hg)
St	=	Strouhal number

Subscripts

LPG = liquefied petroleum gas
LES = Large Eddy Simulation
TKE = Turbulent Kinetic Energy

References

[1] Rayleigh, L.J.R.I.P., *The explanation of certain acoustical phenomena.* J Roy. Inst. Proc., 1878. **8**: p. 536–542.
[2] Putnam, A., et al., *Pulse combustion.* J Progress in energy combustion science, 1986. **12**(1): p. 43–79.
[3] Dec, J.E., et al., *Heat transfer enhancement in the oscillating turbulent flow of a pulse combustor tail pipe.* J International journal of heat mass transfer, 1992. **35**(9): p. 2311–2325.
[4] Dubey, R., et al., *The effect of acoustics on an ethanol spray flame in a propane-fired pulse combustor.* J Combustion Flame, 1997. **110**(1-2): p. 25–38.
[5] Rocha, A.M.A., J.A. Carvalho Jr, and P.T.J.F. Lacava, *Gas concentration and temperature in acoustically excited Delft turbulent jet flames.* J Fuel, 2008. **87**(15–16): p. 3433–3444.
[6] Balachandran, R., et al., *Experimental investigation of the nonlinear response of turbulent premixed flames to imposed inlet velocity oscillations.* J Combustion Flame, 2005. **143**(1–2): p. 37–55.
[7] Liu, X., C. Cao, and Z.J.D.T. Lang, *Heat transfer between materials and unsteady airflow from a Helmholtz type combustor.* J Drying Technology, 2001. **19**(8): p. 1939–1948.
[8] El Behery, R., et al., *Combustion enhancement of a gas flare using acoustical excitation.* Combustion science technology, 2005. **177**(9): p. 1627–1659.
[9] Loretero, M.E., R.F.J.J.o.e.f.g.t. Huang, and power, *Effects of acoustic excitation on a swirling diffusion flame.* Journal of engineering for gas turbines power, 2010. **132**(12).
[10] Hardalupas, Y., A.J.P.i.e. Selbach, and c. science, *Imposed oscillations and non-premixed flames.* J Progress in energy combustion science, 2002. **28**(1): p. 75–104.
[11] Saqr, K.M., et al., *Effect of free stream turbulence on NOx and soot formation in turbulent diffusion CH4-air flames.* J International Communications in Heat Mass Transfer, 2010. **37**(6): p. 611–617.
[12] Kitchen, J.A., *Pulse combustion apparatus*. 1987, Google Patents.

[13] Hamed, A., et al., *Single and Double Flow Pulsations of Normal and Inverse Partially Premixed Methane-Air Flames.* Combustion Science and Technology, 2020: p. 1–31.

[14] Sawarkar, P., T. Sundararajan, and K.J.A.T.E. Srinivasan, *Effects of externally applied pulsations on LPG flames at low and high fuel flow rates.* J Applied Thermal Engineering, 2017. **111**: p. 1664–1673.

[15] Benelli, G., et al., *Advances in numerical simulation of pulsating combustion at ENEL.* J Combustion science technology, 1993. **94**(1–6): p. 317–335.

[16] Mahmoud Magdy, M.M.K., Ashraf M. Hamed, Ahmed Eldein Hussin and Walid Aboelsoud Torky, *Study the Effect of Air Pulsation on the Flame Characteristics.* European Journal of Computational Mechanics, 2021. **29**(2–3): p. 279–302.

[17] Janicka, J. and A.J.P.o.t.C.I. Sadiki, *Large eddy simulation of turbulent combustion systems.* J Proceedings of the Combustion Institute, 2005. **30**(1): p. 537–547.

[18] Pitsch, H.J.A.R.F.M., *Large-eddy simulation of turbulent combustion.* J Annu. Rev. Fluid Mech., 2006. **38**: p. 453–482.

[19] Guo, Z., et al., *Presumed joint probability density function model for turbulent combustion?.* J Fuel, 2003. **82**(9): p. 1091–1101.

[20] Khelil, A., et al., *Prediction of a high swirled natural gas diffusion flame using a PDF model.* J Fuel, 2009. **88**(2): p. 374–381.

[21] Colucci, P., et al., *Filtered density function for large eddy simulation of turbulent reacting flows.* J Physics of Fluids, 1998. **10**(2): p. 499–515.

[22] Jaberi, F., et al., *Filtered mass density function for large-eddy simulation of turbulent reacting flows.* J Journal of Fluid Mechanics, 1999. **401**: p. 85–121.

[23] Dong, L., C.S. Cheung, and C.W.J.E. Leung, *Combustion optimization of a port-array inverse diffusion flame jet.* J Energy, 2011. **36**(5): p. 2834–2846.

[24] Larsson, A., et al., *Skeletal methane–air reaction mechanism for large eddy simulation of turbulent microwave-assisted combustion.* J Energy Fuels, 2017. **31**(2): p. 1904–1926.

[25] Navarro-Martinez, S., et al., *Conditional moment closure for large eddy simulations.* J Flow, Turbulence Combustion, 2005. **75**(1–4): p. 245–274.

[26] Bhaya, R., et al., *Large eddy simulation of mild combustion using pdf-based turbulence–chemistry interaction models.* J Combustion science technology, 2014. **186**(9): p. 1138–1165.

[27] ANSYS, F.I., *Fluent, A.N.S.Y.S Theory Guide 15.* 2013.
[28] Burke, S., T.J.I. Schumann, and E. Chemistry, *Diffusion flames.* J Industrial Engineering Chemistry, 1928. **20**(10): p. 998–1004.
[29] Bilger, R.J.C.s. and technology, *The structure of diffusion flames.* J Combustion science technology, 1976. **13**(1–6): p. 155–170.
[30] Kim, S.H., K.Y.J.C. Huh, and flame, *Second-order conditional moment closure modeling of turbulent piloted jet diffusion flames.* J Combustion flame, 2004. **138**(4): p. 336–352.
[31] Yılmaz, Ý., et al., *Effect of turbulence and radiation models on combustion characteristics in propane–hydrogen diffusion flames.* J Energy conversion management, 2013. **72**: p. 179–186.
[32] Lai, C.H., J.H. Reibenspies, and M.Y.J.A.C.I.E.I.E. Darensbourg, *Thiolate bridged nickel–iron complexes containing both iron (0) and iron (II) carbonyls.* J Angewandte Chemie International Edition in English, 1996. **35**(20): p. 2390–2393.
[33] Liu, T., et al., *Large Eddy Simulation Analysis on Confined Swirling Flows in a Gas Turbine Swirl Burner.* J Energies, 2017. **10**(12): p. 2081.
[34] Dhembare, A.J.A.O.A.S.R., *Bitter truth about fruit with reference to artificial ripener.* J Archives of applied science research, 2013. **5**(5): p. 45–54.
[35] Hosseini, A.A., et al., *Numerical study of inlet air swirl intensity effect of a Methane-Air Diffusion Flame on its combustion characteristics.* J Case Studies in Thermal Engineering, 2020. **18**: p. 100610.
[36] Guessab A., A.A., Baki T., and Bounif A, *The Effects Turbulence Intensity on NOx Formation in Turbulent Diffusion Piloted Flame (Sandia Flame D).* Recent Advances in Mechanical Engineering and Mechanics, 2011. **144–50**.

Biographies

Mahmoud Magdy received the bachelor's degree in mechanical engineering from military technical college in 2012, the master's degree in mechanical power department from Ain shams University in 2018.

Mahmoud Kamal Head of Mechanical Power Engineering Department, Ain Shams University.

Ashraf Mostafa Hamed graduated in 2003 from the Mechanical Power Engineering department at Ain Shams University. He joined the same

department as a demonstrator and finished his MSc in Mechanical Engineering from the same department in 2007. Then, he joined Egypt-Japan University for Science and Technology as PhD student in 2010. Then, he joined Aalto University in Finland as PhD student in 2012. Having obtained his PhD, he was appointed at Ain Shams University in 11/27/2013 as an assistant professor. Currently, He is an associate professor and his research activities are focused on combustion, thermo-fluids, wind energy, turbomachinery, Turbulent Flow Modelling and Computational Fluid Dynamics (CFD).

Ahmed Eldein Hussin is an associate professor at Ain Shams University, Mechanical Power Engineering. His research activities are in the field of thermo-fluid engineering. Currently, he is a co-principal investigator in a joint research project between Ain Shams University and University of Northumbria, the UK, and funded by the British Council and Science & Technology Development Fund. PhD Combustion of Renewable Fuels in Engines, 2013, School of Mech. Eng., Uni. of Leeds, UK. MSc Mechanical Power Engineering, 2006, Faculty of Engineering, Ain Shams University, Egypt. BSc Mechanical Power Engineering, 2001, Faculty of Engineering, Ain Shams University, Egypt. (Distinction with honour degree).

W. Aboelsoud earned his Ph.D. degree from the University of Central Florida, Orlando, FL, USA on May 2013. His research interests are in the advances in renewable energy, energy efficiency and transport phenomena. He is the coordinator of the Mechanical Power Engineering program at Ain Shams University, Cairo, Egypt.